ACS APPLIED ELECTRONIC MATERIALS

ACS AUTHORCHOICE

pubs.acs.org/acsaelm Letter

Tunable Short-Term Plasticity Response in Three-Terminal Organic Neuromorphic Devices

Michele Di Lauro,* Anna De Salvo, Gioacchino Calandra Sebastianella, Michele Bianchi, Stefano Carli, Mauro Murgia, Luciano Fadiga, and Fabio Biscarini

Cite This: *ACS Appl. Electron. Mater.* 2020, 2, 1849−1854

Read Online

ACCESS | Metrics & More | Article Recommendations | Supporting Information

ABSTRACT: Reversibly tunable short-term plasticity (STP) of the channel current in organic neuromorphic devices is demonstrated with a three-terminal architecture. Electrolyte-gated organic transistors—EGOTs—are driven with square voltage pulses at the drain electrodes, while the gate bias enables the modulation of the amplitude and characteristic time scale of the depressive STP spiking response up to 1 order of magnitude. The gate potential sets the baseline and the steady-state current, preluding multilevel memory writing. The fine-tuning of the STP response, which is not possible with two-electrode organic neuromorphic devices, is reversible and does not imply chemical modifications of the active layer.

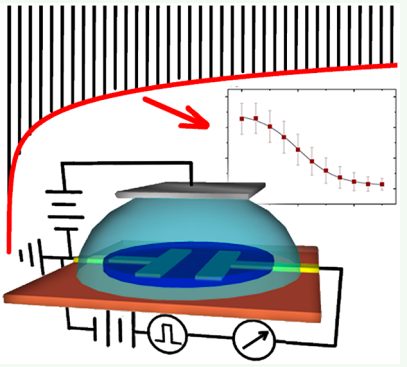

KEYWORDS: *organic neuromorphic device, short-term plasticity, OECT, EGOFET, artificial synapse*

Electronic systems capable of emulating synaptic functionalities, in order to achieve parallel computing with energy efficiency comparable to that of the human brain, were described in 1990 with the locution "neuromorphic electronic systems".[1]

Since then, a number of electronic devices have been designed and developed toward that aim, ranging from memristive circuits,[2,3] in which the resistance state of a semiconductive material (dependent on the past history of the material itself) is used as synaptic weight in artificial neural networks, to asynchronous spiking neural networks, in which information is encoded as spiking time and frequency.[4]

The technological platform of organic electronics, based on inherently low-power devices prone to integration on a large area and capable of working in liquid environment,[5−7] offers unprecedented possibilities in this perspective. Organic neuromorphic devices were successfully demonstrated toward a wide range of applications,[8] ranging from Pavlovian learning to selective sensing of neurotransmitters,[9] as they can reproduce and make advantage of the two main mechanisms characterizing physiological synapses, namely short-term plasticity—STP—and long-term potentiation—LTP.[10] Furthermore, in contrast with their inorganic counterparts, organic neuromorphic devices can be promptly interfaced with living matter and in particular with neural cells,[11] thus becoming an attractive technology for autonomous brain implants and neuroprosthetics.

This work demonstrates the possibility to exploit the peculiar features of electrolyte-gated organic transistors—EGOTs—to develop a new class of three-terminal organic neuromorphic devices that exhibit a reversibly tunable short-term plasticity (STP) response of the channel current.

EGOTs are three-terminal devices in which the current, I_{DS}, that flows in a (semi)conductive channel (i.e., an organic film bridging the source and drain terminals) upon the application of a drain-to-source bias, V_{DS}, is modulated by the voltage applied at the third terminal (the gate) with respect to the source, V_{GS}, as shown in Figure 1. The gate is capacitively coupled to the organic film through an electrolyte; hence, V_{GS} modulates channel conductance by controlling the ionic environment and potential in the proximity to the channel.[12−16]

Usually, when organic transistor architectures are operated to yield a neuromorphic response, two of the three terminals are short-circuited together, obtaining a *de facto* two-terminal architecture,[17] whose time/frequency response reflects an effective RC time constant of the circuit. This time constant depends on geometrical features such as channel thickness,[18] on the judicious integration of shallow traps, for instance, those made with Au nanoparticles,[19] or on the composition of the electrolyte or the presence of molecules strongly interacting with the active layer. In particular, the latter case allowed the use of

Received: April 19, 2020
Accepted: July 7, 2020
Published: July 7, 2020

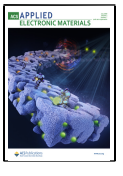

https://dx.doi.org/10.1021/acsaelm.0c00313
ACS Appl. Electron. Mater. 2020, 2, 1849−1854

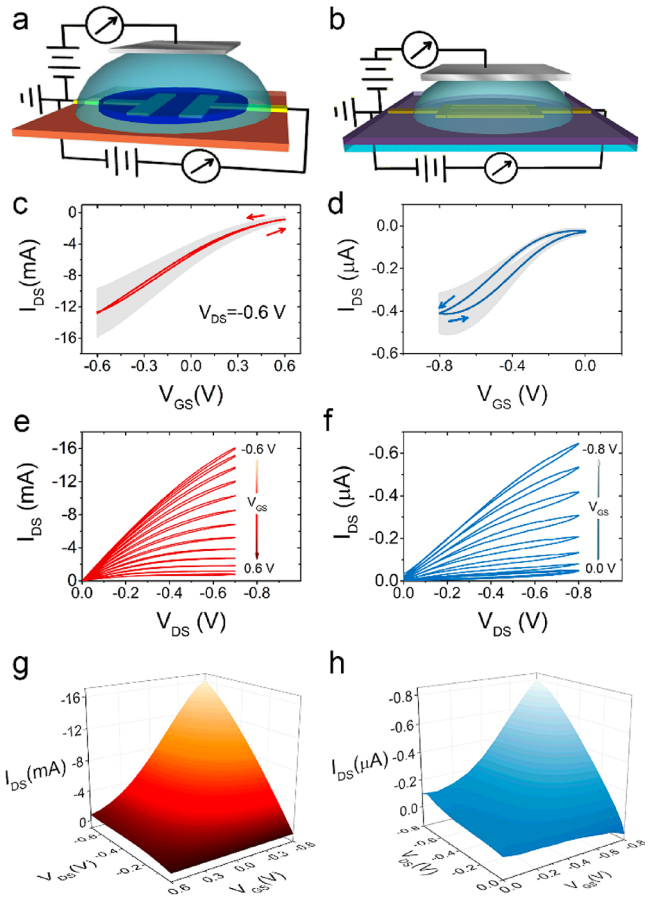

Figure 1. (a,b) Schematic representation and connection layout of the proposed PEDOT:PSS-based depletion EGOT (a) and TIPS–pentacene accumulation EGOT (b), operated in a common source–common ground configuration; (c,d) average transfer characteristics of depletion (c) and accumulation (d) devices, reported with their SEM (N = 5, gray area); (e,f) typical output characteristics of depletion (e) and accumulation (f) devices; (g,h) 3-D plots showing the dependence of I_{DS} from both V_{GS} and V_{DS}, for depletion (g) and accumulation (h) devices.

STP timescales as a sensing parameter toward analytes in the electrolyte exhibiting strong (from a few to several tens kJ mol^{-1}), albeit nonspecific, interactions with the active material.[20] In all these approaches, depressive STP is obtained when the voltage spike train has a frequency higher than the inverse of the device response characteristic time scale, which is largely contributed by the resistance–capacitance of the electrolyte/active material interface.

In other three-terminal approaches,[21−24] STP has been achieved in poly(3,4-ethylenedioxythiophene):polystyrenesulfonate (PEDOT:PSS)-based or poly(3-hexylthiophene) (P3HT)-based EGOTs by continuously recording I_{DS} while applying pulses at the gate electrode and exploiting the rather slow bulk dedoping/doping of semiconductive channels to achieve nonlinearity of the I_{DS} response according to the stimulation frequency. LTP, on the other hand, has been achieved by faradaic processes such as lithium intercalation in the channel of graphene FETs.[25]

In this work, a novel EGOT-based neuromorphic architecture is reported, in which the doping state of the channel is kept constant throughout the entire stimulation protocol by applying a constant V_{GS}. An STP depressive response of I_{DS} is observed upon V_{DS} square pulsing, achieving selective and reversible tuning of STP behavior via V_{GS}-mediated control of channel doping. Importantly, the gate voltage does not produce any redox reaction in the active layer. The rationale is that eliciting STP modulation of I_{DS} by square pulse V_{DS} stimulation, it is possible to exploit V_{GS} as an additional tuning parameter, to modulate charge carrier density in the semiconductive channel, regulating both the STP amplitude and STP time constant at the same time. The gate also allows the baseline current to be set before and at the steady state after the STP response, thus acting as a further element for memory writing.

Depletion and accumulation EGOTs were fabricated using PEDOT:PSS and 6,13-bis(triisopropylsilylethynyl)pentacene (TIPS-P5), respectively, and characterized with standard protocols,[26] in order to assess the feasibility and the reproducibility of the proposed strategy. The results are summarized in Figure 1.

Transfer (Figure 1c,d) and output (Figure 1e,f) characteristics confirmed that PEDOT:PSS-based EGOTs exhibit higher absolute I_{DS} values compared to TIPS-P5-based devices. Nevertheless, as shown in Figure 1g,h, in both architectures, it is possible to reversibly shift from a high-conductance state to a low-conductance state when scanning V_{GS} from negative to positive values; this common feature has been exploited to tune the STP depressive response in both architectures.

A schematic representation of the connection layout is presented in Figure 2a.

The envisioned stimulation protocol was validated by sourcing square pulse trains of varying frequencies at the drain electrode following the established stimulation pattern[27] while applying a constant DC bias V_{GS} at the gate and keeping a fixed nonzero drain bias ($V_{DS,0}$ = −0.3 V). Figure 2b shows the stimulation protocol and the response of a three-terminal STP device obtained in a depletion PEDOT:PSS-based EGOT architecture: upon channel dedoping (i.e., when moving from negative V_{GS} values to positive values), it is possible to observe a decrease of the current spike amplitude. This is consistent with the profile of the transfer characteristics (shown in Figure 1c), which is also mirrored by the trend of the DC current in absence of stimulation.

The typical response of neuromorphic two-terminal devices is qualitatively retained: it is possible to observe a linear response at low frequencies, a depressing response at high frequencies, and a facilitating response (viz., current spike amplitude increasing) when moving from high to low frequencies. Nonetheless, in a three-terminal architecture, it is possible to modulate this behavior, at least until the neuromorphic response for completely dedoped channels (i.e., V_{GS} = 0.6 V) is suppressed. This behavior arises from the different nature of charge carriers contributing to I_{DS} in response to V_{DS} pulses: namely, holes in the semiconductive channel (slow carriers) and ions displacing in the electrolyte (fast carriers). When the channel is completely dedoped, holes are trapped, and I_{DS} is due to mere ion displacement, resulting in lower current intensity and faster relaxation timescales. In this scenario, the stimulation frequency is not high enough to elicit depression, and the device response will be linear. This effect is displayed in Figure 2c, showing the current variations ΔI_{DS} in response to individual V_{DS} square waves in the "depressive" region. Besides the aforementioned decrease of intensity, it is possible to observe significant evolution of the relaxation time-scales exhibited by the system when pulses are applied and removed. Interestingly, it is possible to decouple these two phenomena (pulse

https://dx.doi.org/10.1021/acsaelm.0c00313
ACS Appl. Electron. Mater. 2020, 2, 1849−1854

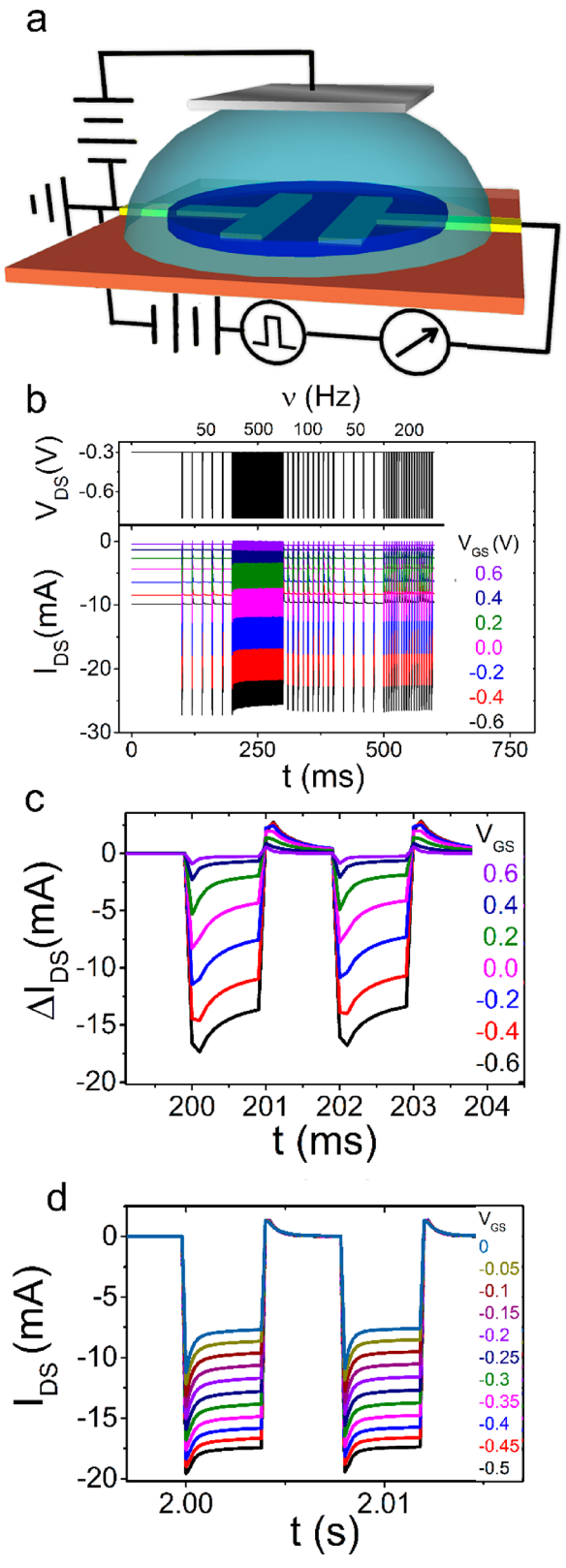

Figure 2. (a) Connection layout for eliciting a tunable STP response: a constant gate bias is applied, while at the drain terminal, voltage pulses are applied, and I_{DS} is recorded; (b) response of the accumulation EGOT to a V_{DS} pulse train ($V_{DS,0}$ = −0.3 V; ΔV_{DS} = −0.5 V) at different V_{GS} values; (c) detail of I_{DS} variations in the depressive region of (b) at 500 Hz, highlighting the dependency of both spike amplitude and relaxation time scales on V_{GS}; (d) system response to depressive stimulation frequency (125 Hz) for $V_{DS,0}$ = 0 V, for −0.5 < V_{GS} < 0 V.

application and pulse removal) if no DC drain bias is applied (i.e., if $V_{DS,0}$ = 0 V), as shown in Figure 2d.

In order to define the operational parameters necessary for predicting and tailoring the STP response in a three-terminal device, it is necessary to develop a quantitative toolset that rationalizes these phenomena. In this work, this has been done by focusing on the STP depressive response at 125 Hz at $V_{DS,0}$ = 0 V, for V_{GS} values ranging to 0 V to −0.5 V, since within this potential window, it is possible to modulate the conductivity of the large majority of p-type organic semiconductors and to rule out any faradaic contribution to the observed currents.[28]

The typical STP depressive response, characterized by a decreasing envelope of the current maxima in response to subsequent voltage spikes (shown in Figure 3a,b), follows the stretched exponential trend of eq 1:

$$I(t) = I_\infty + A\cdot\exp\left[-\left(\frac{\Delta t}{\tau_{STP}}\right)^\beta\right] \quad (1)$$

where I_∞ is the current plateau related to the equilibrium reached upon continuous depressive stimulation, $A = I_0 - I_\infty$ is the difference between the first spike, I_0, and I_∞, $\Delta t = t - t_0$ is the time interval from the first spike, τ_{STP} is the STP time scale, and the exponent, β, quantifies the deviation from the exponential trend (which is instead usually observed in two-terminal devices).[29] Figure 3c shows the trends of I_∞ and A vs V_{GS} for depletion EGOTs, while Figure 3d reports the same trends for accumulation devices. In depletion devices, the increasing trend of I_∞ for higher channel doping (i.e., more negative V_{GS} and higher negative I_∞) is mirrored by a decrease in STP amplitude, A. This is due to the fact that, for negative V_{GS}, conduction in PEDOT:PSS approaches metallic conduction, resulting in a partial loss of tunability. In accumulation devices, on the other hand, the active material is completely undoped at V_{GS} = 0 and is populated by charge carriers while moving at a more negative V_{GS}; in this situation, the amplitude of the STP modulation, A, and the plateau current, I_∞, follow exactly the same trend vs V_{GS}. This shows that V_{GS} also controls current baseline.

The stretching exponent, β (plotted vs V_{GS} in Figure 3g,h for depletion and accumulation devices, respectively), is a measure of the deviation from the ideal exponential STP decay. In the three-terminal architecture, the observed β < 1 produces a less steep decay. This hints to energetic disorder and dispersion of drift velocities in semiconductive channels, and it is different from displacement-based STP in two-terminal architectures, where β = 1. Also, β dependency on V_{GS} differs for depletion and accumulation devices. In the former, it increases with channel doping and approaches unity, resulting in steeper decays; in the latter, it increases linearly in the subthreshold operational regime (−0.2 < V_{GS} < 0 V, where the channel gets populated) and remains rather constant in the linear accumulation regime.

Since the sampled time for a train of voltage pulses may be shorter than the STP time scale (in some instances, this falls outside the range of experimental time, which means the plateau of STP is not fully achieved for the duration of the pulse train), the estimated errors on the fitting parameters are large, and convergence requires a step-and-hold fitting procedure. Thus, we recast eq 1 and perform its Taylor expansion into a power law

$$I(t) \approx I_0 + I_\infty\cdot\left(\frac{\Delta t}{\tau_{STP}}\right)^\beta \quad (2)$$

which can be linearized as

https://dx.doi.org/10.1021/acsaelm.0c00313
ACS Appl. Electron. Mater. 2020, 2, 1849−1854

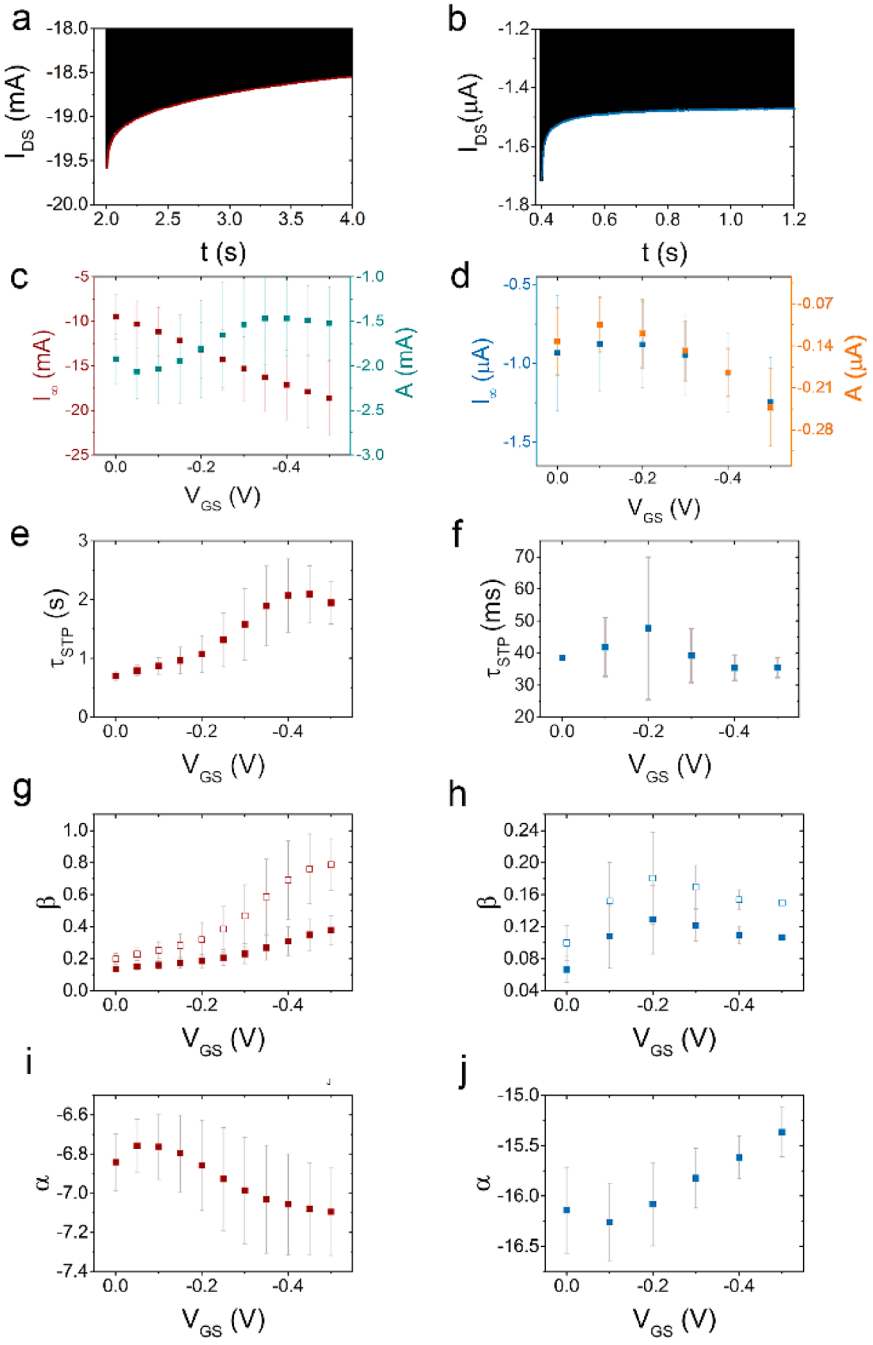

Figure 3. (a,b) Typical depressive STP responses (solid black line) and STP envelopes (solid red and blue lines) for depletion (a) and accumulation (b) devices; (c,d) dependency of current plateau, I_∞, and STP amplitude, A, on V_{GS}, for depletion (c) and accumulation (d) devices; (e,f) dependency of STP time scale, τ_{STP}, on V_{GS}, for depletion (e) and accumulation (f) devices; (g,h) dependency of stretching exponent, β, as extracted from the stretched exponential trend (hollow squares) and from the linearized one (solid squares) on V_{GS}, for depletion (g) and accumulation (h) devices; (i,j) dependency of the linearized trends slope, α, on V_{GS}, for depletion (i) and accumulation (j) devices.

$$\ln\left[\frac{I(t)-I_0}{1A}\right] = \left[\ln\left(\frac{I_\infty}{1A}\right) - \beta\cdot\ln\left(\frac{\tau_{STP}}{1s}\right)\right] + \beta\cdot\ln\left(\frac{\Delta t}{1s}\right) = \alpha + \beta\cdot\ln\left(\frac{\Delta t}{1s}\right) \quad (3)$$

The fit with eq 3 is numerically robust, although the physical meaning of the parameters of eq 2 is not explicit, as the parameters are now entangled into the parameter α, which is plotted vs V_{GS} in Figure 3i,j. The linearization procedure also leads to a slight underestimation of β values, as shown in Figure 3g,h.

As already discussed, both α and β can be tuned by controlling V_{GS}.

The parameter α, namely the value of $\ln\left[\frac{\Delta I(t)}{1A}\right]$ after 1 s of continuous depressive stimulation, is a generic indicator of the efficiency of the STP depression. Indeed, in depletion devices, α exhibits a maximum at V_{GS} close to 0 V, where the channel is in its most energetically disordered state (see also Figure 1c for comparison). Accordingly, β is at a minimum in this potential window.

https://dx.doi.org/10.1021/acsaelm.0c00313
ACS Appl. Electron. Mater. 2020, 2, 1849−1854

In accumulation EGOTs, Figure 3j, the trend is exactly reversed, since these devices experience the opposite transition, i.e., from insulating to conductive, while moving toward negative V_{GS} values; thus, their STP efficiency scales directly with the charge carrier density.

As complementary information to this framework, it is worth noticing that τ_{STP}—namely the time constant of the I_{DS} decay upon depressive stimulation—is different than the circuit RC time constant, τ, extracted from impedance spectroscopy (Figure S1 in the Supporting Information). In particular, devices with faster relaxation (i.e., smaller τ) exhibit a longer τ_{STP}. This is not surprising if one considers the fact that STP arises from incomplete relaxation of the system upon continuous spiking: namely, at a given stimulation frequency, in a system with a smaller τ, the intensity of the second spike will be closer to that of the first spike if compared to what would happen in a slower system (bigger τ), resulting in the need of more spikes (i.e., longer times) to reach a steady state, causing a longer τ_{STP}.

In conclusion, a novel neuromorphic architecture based on electrolyte-gated organic transistors (working either in depletion or in accumulation) was developed and validated, allowing reversible tuning of the amplitude, rate, and current plateau of the neuromorphic depressive response upon V_{GS} modulation. By properly controlling V_{GS}, it is possible to shift the baseline current, the amplitude, and the steepness of neuromorphic behavior in the channel of organic electronic EGOT-based neuromorphic devices, preluding multilevel memory writing and frequency dependent controllable decisional nodes in more complex neuromorphic organic circuitry as well as tailorable sensitivity in STP-based sensors.

EXPERIMENTAL SECTION

Depletion EGOT Fabrication. Custom test patterns were designed and purchased by Phoenix PCB. The final design features nine independent pairs of gold source/drain electrodes ($W/L = 4$) patterned onto a flexible poly imide substrate. Insulation is guaranteed by a further polyimide layer, which covers the entire layout and features nine pools that expose only the terminal portion (area = 0.8 × 0.9 mm) of the source and drain leads. Semiconductive channels are obtained by dropcasting 0.5 μL of a PEDOT:PSS formulation (Clevios PH1000, 5% v/v DMSO, 0.2% v/v GOPS; diluted 10 times with Milli-Q water) on each pool and curing in a thermostatic oven (120 °C, 30 min) obtaining films with an average 1 μm thickness (XE7 AFM Park System, tapping mode).

Accumulation EGOT Fabrication. Au source and drain interdigitated electrodes were deposited onto quartz substrates by photolithography and liftoff (MicroFabSolutions, Trento, Italy), obtaining a 15 μm long and 3 mm wide channel. TIPS-P5 was deposited after piranha wet etch (1:1, H_2SO_4/H_2O_2) treatment onto these substrates via spin coating of a 1% w/w solution in an 8:2 mixture of toluene and *n*-hexane and cured in a thermostatic oven (60 °C, 30 min).

Device Characterization. Device performances have been assessed using a two-channel source measure unit—SMU (Keysight, B2912A)—with custom designed control software. In particular, $I-V$ characteristics have been acquired in the usual common source–common ground configuration, while neuromorphic tunable behavior has been obtained driving the pulsed drain electrode with one channel of the SMU, using the other channel to provide a DC bias at the gate electrode.

ASSOCIATED CONTENT

Supporting Information

The Supporting Information is available free of charge at https://pubs.acs.org/doi/10.1021/acsaelm.0c00313.

Impedance spectroscopy of the channel at various V_{GS} values; RC time constant, τ, vs V_{GS} (PDF)

AUTHOR INFORMATION

Corresponding Author

Michele Di Lauro − *Center for Translational Neurophysiology of Speech and Communication, Fondazione Istituto Italiano di Tecnologia (IIT-CTNSC), 44121 Ferrara, Italy;* orcid.org/0000-0002-7072-9468; Email: michele.dilauro@iit.it

Authors

Anna De Salvo − *Center for Translational Neurophysiology of Speech and Communication, Fondazione Istituto Italiano di Tecnologia (IIT-CTNSC), 44121 Ferrara, Italy; Sezione di Fisiologia Umana, Università di Ferrara, 44121 Ferrara, Italy;* orcid.org/0000-0001-6669-9115

Gioacchino Calandra Sebastianella − *Dipartimento di Scienze Biomediche, Metaboliche e Neuroscienze, Università di Modena e Reggio Emilia, 41125 Modena, Italy*

Michele Bianchi − *Center for Translational Neurophysiology of Speech and Communication, Fondazione Istituto Italiano di Tecnologia (IIT-CTNSC), 44121 Ferrara, Italy;* orcid.org/0000-0002-9660-9894

Stefano Carli − *Center for Translational Neurophysiology of Speech and Communication, Fondazione Istituto Italiano di Tecnologia (IIT-CTNSC), 44121 Ferrara, Italy;* orcid.org/0000-0002-0309-2356

Mauro Murgia − *Center for Translational Neurophysiology of Speech and Communication, Fondazione Istituto Italiano di Tecnologia (IIT-CTNSC), 44121 Ferrara, Italy; Istituto per lo Studio dei Materiali Nanostrutturati (CNR-ISMN), National Research Council, 40129 Bologna, Italy*

Luciano Fadiga − *Center for Translational Neurophysiology of Speech and Communication, Fondazione Istituto Italiano di Tecnologia (IIT-CTNSC), 44121 Ferrara, Italy; Sezione di Fisiologia Umana, Università di Ferrara, 44121 Ferrara, Italy*

Fabio Biscarini − *Center for Translational Neurophysiology of Speech and Communication, Fondazione Istituto Italiano di Tecnologia (IIT-CTNSC), 44121 Ferrara, Italy; Dipartimento di Scienze della Vita, Università di Modena e Reggio Emilia, 41125 Modena, Italy*

Complete contact information is available at: https://pubs.acs.org/10.1021/acsaelm.0c00313

Author Contributions

The manuscript was written through contributions of all authors.

Notes

The authors declare no competing financial interest.

ACKNOWLEDGMENTS

Research work leading to this publication has been funded by the IIT-Italian Institute of Technology, University of Ferrara, University of Modena and Reggio Emilia and Institute for the Study of Nanostructured Materials of the Italian National Research Council (CNR-ISMN).

ABBREVIATIONS

STP, Short-term plasticity
LTP, Long-term potentiation
EGOT, Electrolyte-gated organic transistor

https://dx.doi.org/10.1021/acsaelm.0c00313
ACS Appl. Electron. Mater. 2020, 2, 1849−1854

PEDOT:PSS, poly(3,4-ethylenedioxythiophene):polystyrenesulfonate
TIPS-P5, 6,13-bis(triisopropylsilylethynyl)pentacene
P3HT, poly(3-hexylthiophene)

REFERENCES

(1) Mead, C. Neuromorphic Electronic Systems. *Proc. IEEE* **1990**, *78* (10), 1629−1636.
(2) Chua, L. Memristor - The Missing Circuit Element. *IEEE Trans. Circuit Theory* **1971**, *18* (5), 507−519.
(3) Strukov, D. B.; Snider, G. S.; Stewart, D. R.; Williams, R. S. The Missing Memristor Found. *Nature* **2008**, *453* (7191), 80−83.
(4) Burr, G. W.; Shelby, R. M.; Sebastian, A.; Kim, S.; Kim, S.; Sidler, S.; Virwani, K.; Ishii, M.; Narayanan, P.; Fumarola, A.; Sanches, L. L.; Boybat, I.; Le Gallo, M.; Moon, K.; Woo, J.; Hwang, H.; Leblebici, Y. Neuromorphic Computing Using Non-Volatile Memory. *Adv. Phys. X* **2017**, *2* (1), 89−124.
(5) Someya, T.; Bao, Z.; Malliaras, G. G. The Rise of Plastic Bioelectronics. *Nature* **2016**, *540* (7633), 379−385.
(6) Malliaras, G. G. Organic Bioelectronics: A New Era for Organic Electronics. *Biochim. Biophys. Acta, Gen. Subj.* **2013**, *1830* (9), 4286−4287.
(7) Simon, D. T.; Gabrielsson, E. O.; Tybrandt, K.; Berggren, M. Organic Bioelectronics: Bridging the Signaling Gap between Biology and Technology. *Chem. Rev.* **2016**, *116*, 13009−13041.
(8) Van De Burgt, Y.; Melianas, A.; Keene, S. T.; Malliaras, G.; Salleo, A. Organic Electronics for Neuromorphic Computing. *Nature Electronics* **2018**, *1*, 386−397.
(9) Giordani, M.; Di Lauro, M.; Berto, M.; Bortolotti, C. A.; Vuillaume, D.; Gomes, H. L.; Zoli, M.; Biscarini, F. Whole Organic Electronic Synapses for Dopamine Detection. *Proc. SPIE* **2016**, *9944*, 99440P.
(10) Martin, S. J.; Grimwood, P. D.; Morris, R. G. M. SYNAPTIC PLASTICITY AND MEMORY: An Evaluation of the Hypothesis. *Annu. Rev. Neurosci.* **2000**, *23*, 649−711.
(11) Desbief, S.; Di Lauro, M.; Casalini, S.; Guerin, D.; Tortorella, S.; Barbalinardo, M.; Kyndiah, A.; Murgia, M.; Cramer, T.; Biscarini, F.; et al. Electrolyte-Gated Organic Synapse Transistor Interfaced with Neurons. *Org. Electron.* **2016**, *38*, 21−28.
(12) Wang, D.; Noël, V.; Piro, B. Electrolytic Gated Organic Field-Effect Transistors for Application in Biosensors—A Review. *Electronics* **2016**, *5*, 9.
(13) Bernards, D. A.; Malliaras, G. G. Steady-State and Transient Behavior of Organic Electrochemical Transistors. *Adv. Funct. Mater.* **2007**, *17* (17), 3538−3544.
(14) Di Lauro, M.; Casalini, S.; Berto, M.; Campana, A.; Cramer, T.; Murgia, M.; Geoghegan, M.; Bortolotti, C. A.; Biscarini, F. The Substrate Is a PH-Controlled Second Gate of Electrolyte-Gated Organic Field-Effect Transistor. *ACS Appl. Mater. Interfaces* **2016**, *8* (46), 31783−31790.
(15) Giovannitti, A.; Sbircea, D.-T.; Inal, S.; Nielsen, C. B.; Bandiello, E.; Hanifi, D. A.; Sessolo, M.; Malliaras, G. G.; McCulloch, I.; Rivnay, J. Controlling the Mode of Operation of Organic Transistors through Side-Chain Engineering. *Proc. Natl. Acad. Sci. U. S. A.* **2016**, *113* (43), 12017−12022.
(16) Di Lauro, M.; Berto, M.; Giordani, M.; Benaglia, S.; Schweicher, G.; Vuillaume, D.; Bortolotti, C. A.; Geerts, Y. H.; Biscarini, F. Liquid-Gated Organic Electronic Devices Based on High-Performance Solution-Processed Molecular Semiconductor. *Adv. Electron. Mater.* **2017**, *3* (9), 1700159.
(17) Alibart, F.; Pleutin, S.; Guérin, D.; Novembre, C.; Lenfant, S.; Lmimouni, K.; Gamrat, C.; Vuillaume, D. An Organic Nanoparticle Transistor Behaving as a Biological Spiking Synapse. *Adv. Funct. Mater.* **2010**, *20* (2), 330−337.
(18) Gerasimov, J. Y.; Gabrielsson, R.; Forchheimer, R.; Stavrinidou, E.; Simon, D. T.; Berggren, M.; Fabiano, S. An Evolvable Organic Electrochemical Transistor for Neuromorphic Applications. *Adv. Sci.* **2019**, *6* (7), 1801339.
(19) Desbief, S.; Di Lauro, M.; Casalini, S.; Guerin, D.; Tortorella, S.; Barbalinardo, M.; Kyndiah, A.; Murgia, M.; Cramer, T.; Biscarini, F.; Vuillaume, D. Electrolyte-Gated Organic Synapse Transistor Interfaced with Neurons. *Org. Electron.* **2016**, *38*, 21−28.
(20) Giordani, M.; Berto, M.; Di Lauro, M.; Bortolotti, C. A.; Zoli, M.; Biscarini, F. Specific Dopamine Sensing Based on Short-Term Plasticity Behavior of a Whole Organic Artificial Synapse. *ACS Sensors* **2017**, *2* (12), 1756−1760.
(21) Gkoupidenis, P.; Schaefer, N.; Garlan, B.; Malliaras, G. G. Neuromorphic Functions in PEDOT:PSS Organic Electrochemical Transistors. *Adv. Mater.* **2015**, *27* (44), 7176−7180.
(22) Qian, C.; Sun, J.; Kong, L. A.; Gou, G.; Yang, J.; He, J.; Gao, Y.; Wan, Q. Artificial Synapses Based on In-Plane Gate Organic Electrochemical Transistors. *ACS Appl. Mater. Interfaces* **2016**, *8* (39), 26169−26175.
(23) Ling, H.; Koutsouras, D. A.; Kazemzadeh, S.; Van De Burgt, Y.; Yan, F.; Gkoupidenis, P. Electrolyte-Gated Transistors for Synaptic Electronics, Neuromorphic Computing, and Adaptable Biointerfacing. *Appl. Phys. Rev.* **2020**, *7* (1), 011307.
(24) Hu, Y.; Zeng, F.; Chang, C.; Dong, W.; Li, X.; Pan, F.; Li, G. Diverse Synaptic Plasticity Induced by the Interplay of Ionic Polarization and Doping at Salt-Doped Electrolyte/Semiconducting Polymer Interface. *ACS Omega* **2017**, *2* (2), 746−754.
(25) Sharbati, M. T.; Du, Y.; Torres, J.; Ardolino, N. D.; Yun, M.; Xiong, F. Low-Power, Electrochemically Tunable Graphene Synapses for Neuromorphic Computing. *Adv. Mater.* **2018**, *30*, 1802353.
(26) IEEE. *Standard Test Methods for the Characterization of Organic Transistors and Materials*; IEEE Std 1620−2004; 2004. https://ieeexplore.ieee.org/document/1293918.
(27) Desbief, S.; Kyndiah, A.; Guérin, D.; Gentili, D.; Murgia, M.; Lenfant, S.; Alibart, F.; Cramer, T.; Biscarini, F.; Vuillaume, D. Low Voltage and Time Constant Organic Synapse-Transistor. *Org. Electron.* **2015**, *21*, 47−53.
(28) Cramer, T.; Campana, a.; Leonardi, F.; Casalini, S.; Kyndiah, a.; Murgia, M.; Biscarini, F. Water-Gated Organic Field Effect Transistors − Opportunities for Biochemical Sensing and Extracellular Signal Transduction. *J. Mater. Chem. B* **2013**, *1* (31), 3728.
(29) Giordani, M.; Sensi, M.; Berto, M.; Di Lauro, M.; Bortolotti, C. A.; Gomes, H. L.; Zoli, M.; Zerbetto, F.; Fadiga, L.; Biscarini, F. Neuromorphic Organic Devices That Specifically Discriminate Dopamine from Its Metabolites by Nonspecific Interactions. *Adv. Funct. Mater.* **2020**, 2002141.

https://dx.doi.org/10.1021/acsaelm.0c00313
ACS Appl. Electron. Mater. 2020, 2, 1849−1854